analytical chemistry

Article

pubs.acs.org/ac

Using A Fiber Optic Particle Plasmon Resonance Biosensor To Determine Kinetic Constants of Antigen–Antibody Binding Reaction

Ting-Chou Chang,[†,§] Chao-Ching Wu,[†,§] Shau-Chun Wang,*[,†,§] Lai-Kwan Chau,*[,†,§] and Wen-Hsin Hsieh[‡,§]

[†]Department of Chemistry and Biochemistry, [‡]Department of Mechanical Engineering, and [§]Center for Nano Bio-Detection, National Chung Cheng University, 168 University Road, Min-Hsiung, Chia-Yi 621, Taiwan

ABSTRACT: In this paper, one simple and label-free biosensing method has been developed for determining the binding kinetic constants of antiovalbumin antibody (anti-OVA) and anti-mouse IgG antibody using the fiber optic particle plasmon resonance (FOPPR) biosensor. The FOPPR sensor is based on gold-nanoparticle-modified optical fiber, where the gold nanoparticle surface has been modified by a mixed self-assembled monolayer for conjugation of a molecular probe reporter (ovalbumin or mouse IgG) to dock with the corresponding analyte species such as anti-OVA or anti-mouse IgG. The binding process, occurring when an analyte reacts with a probe molecule immobilized on the optical fiber, can be monitored in real-time. In addition, by assuming a Langmuir-type adsorption isotherm to measure the initial binding rate, the quantitative determination of binding kinetic constants, the association and dissociation rate constants, yields k_a of $(7.21 \pm 0.4) \times 10^3$ M^{-1} s^{-1} and k_d of $(2.97 \pm 0.1) \times 10^{-3}$ s^{-1} for OVA/anti-OVA and k_a of $(1.45 \pm 0.2) \times 10^6$ M^{-1} s^{-1} and k_d of $(2.97 \pm 0.6) \times 10^{-2}$ s^{-1} for mouse IgG/anti-mouse IgG. We demonstrate that the FOPPR biosensor can study real-time biomolecular interactions.

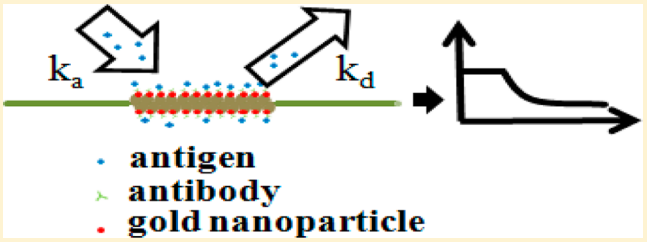

A number of research groups have reported pioneering results to investigate the potential of nanoscale sensors for label-free detection of biomolecules in order to study immunobinding kinetic without altering the structure of ducking functionalities.[1−5] Nanoparticles of noble metal such as gold characteristically exhibit a strong absorption band that does not appear in the spectrum of the bulk metal. The light absorption of this characteristic band is the consequence of the incident photon frequency being resonant with the collective oscillation of the conduction electrons. This phenomenon is known as localized surface plasmon resonance (LSPR), also known as particle plasmon resonance (PPR). The resonance frequency of the PPR considerably shifts when even tiny change in the nanoparticle's local environment occurs.[6,7] The optical properties, such as absorbance and peak wavelength, of noble metal nanoparticles are highly susceptible to the refractive index (RI) of the surrounding medium and, additionally, the molecule docking events to those functionalized nanoparticles.[1,2,8−10] Besides, the detection is label-free without altering the docking functionalities, and the binding event can be monitored concurrently with high sensitivity by using simple, cost-effective equipment.[1,8] The biosensor has a similar[11] or even better[12,13] response as compared to a commercial surface plasmon resonance (SPR) instrument (based on propagating plasmons in a thin gold film) and shows less interference from bulk RI.[14] The sensitivity of the PPR sensor can be further enhanced by a fiber optic evanescent-wave approach, where an optimized length of the unclad portion of an optical fiber has been coated with noble metal nanoparticles, usually implanted with molecular probes.[1] It has been demonstrated that the sensing sensitivity is dependent on the length of the sensing fiber.[12,15]

Biosensing methods have been a conventional means to measure the binding affinity and rate constants of immunological reactions.[16] Recently, a biosensing method has also been employed to screen drug candidates.[17] In particular, the quantitative investigation of binding kinetics provides important information regarding cell adhesion mechanisms during immunoresponse processes and the interactions between the docking target molecule and the counterpart probe molecule. Besides, the functional or conformational changes of target proteins can be revealed by the variation of binding affinity and rate constants. Binding affinity constants can be measured when the docking between antigen and antibody reaches equilibrium. However, temporal concentration changes of each immunoassay species are required to be monitored in order to determine the binding rate constants. Although fluorescence or radioactive tags have been used to label investigated molecules to monitor temporal concentration changes, the inevitable property alterations due to chemical modification on the molecules often result in inaccurate estimations of binding kinetic constants.[18] A label-free method can therefore remedy this problem inherent in conventional methods.

In this paper, the sensing chip made of polymeric substrate contains a flow cell channel of dimensions 15 mm × 1 mm × 1

Received: September 7, 2012
Accepted: November 27, 2012
Published: November 27, 2012

   dx.doi.org/10.1021/ac302590n | *Anal. Chem.* 2013, 85, 245−250

mm. A partially unclad optical fiber is then placed in the channel. In our experiments, antigen is immobilized on the fiber surface as probe molecule. And then, the target molecule antibody is infused into the flow cell to contact with the antigen on the fiber surface. The reaction dynamics between antigen and antibody can be monitored with the temporal change of signal intensity. This transient intensity evolution can be plotted as a sensorgram.

In the above antigen−antibody interaction model, the formation of antigen−antibody complex on the fiber surface can be described as

$$\mathrm{Ag} + \mathrm{Ab} \underset{k_d}{\overset{k_a}{\rightleftarrows}} \mathrm{Ag{:}\,Ab} \quad (1)$$

where Ag and Ab represent the reactant species, antigen and antibody, respectively, and the product complex is denoted as Ag:Ab. In eq 1, k_a and k_d are the association rate constant and the dissociation rate constant, respectively, governing the formation of product complex. Since the immobilized antigen docks with antibody to form immobilized product complex, the model in eq 1 is similar to the Langmuir isotherm when the product complex is assumed to pile as a monolayer.

In the beginning of binding reaction, the kinetics rate equation is assumed to follow pseudo-first-order approximation. Under the boundary conditions of reaching binding steady state at infinite time, when fiber optic particle plasmon resonance (FOPPR) signal intensity $I_{(t)}$ is proportional the surface concentration of antibody−antigen complex on the coated layer, one linear relation of the logarithm value $\ln[(I_{(t)} - I_{eq})/(I_o - I_{eq})]$ versus time t can be obtained, where I_{eq} and I_o represent the signal intensity at initial and infinite times, respectively. The procedure to derive this relation is illustrated in detail in the Materials and Methods. Besides, the slope of this relation scales with $k_aC + k_d$, where C is the concentration of loaded antibody samples. Therefore, using a series of concentrations of antibody, the regression of slope against concentrations can result in the binding kinetics constants k_a and k_d.

Many biosensing methods for determining kinetic rates involve stepwise titration[19−21] or kinetic analysis in which the sensor signal is monitored as a function of time after analyte injection.[22,23] For systems exhibiting slow kinetics, a full titration experiment may take several hours to complete. During that time, biological molecules may denature, making it difficult to interpret the resulting data. On the other hand, kinetic experiments can be performed very quickly, but they must be repeated at multiple flow rates and analyte concentrations to ensure accurate results and to isolate the effect of mass transport.[24−26] If the reaction is partially irreversible, the dissociation rate is extremely slow and thus regeneration of the sensor can be extremely difficult.

In our method, the sample is quickly loaded (less than 5 s) into the sensing cell for the analyte to park statically while recording the binding process, which completes in 100 s at least. In contrast, using another type of flow cell device such as a Biacore surface plasmon resonance (SPR) chip, the reaction kinetics measurement is limited by the flow rate of sample loading, because fast association is completed as soon as the sample filled the thin sensing cell of very short solute diffusion distance. Unlike using the SPR chip, the FOPPR sensing cell is able to measure any binding rate because the sample loading takes less than $^1/_{10}$ of the binding duration, typically $^1/_{100}$ or even less. So the initial binding rate in a FOPPR cell is only controlled by sample concentration to estimate the binding association constant k_a.

According to this passage, the binding process is recorded in static mode when analyte solution is loaded in one static sensing cell. Unlike using a flow cell device like a SPR chip, the kinetic rate constant measurement is not limited by sample flow rate. The ability to analyze biomolecules without flow may be especially useful when an experimentalist only has a small amount of analyte available to characterize a biomolecular interaction.

MATERIALS AND METHODS

Reagents. The following reagent-grade chemicals were purchased from Sigma-Aldrich (St. Louis, MO): 11-mercaptoundecanoic acid (MUA), 6-mercapto-1-hexanol (MCH), *N*-hydroxysuccinimide (NHS), 1-ethyl-3-(3-dimethylaminopropyl)carbodiimine hydrochloride (EDC), and ethanolamine. (3-Mercaptopropyl)trimethoxysilane (MPTMS, 98%) and cetyltrimethylammonium bromide (CTAB) were obtained from Acros. Hydrogen tetrachloroaurate trihydrate ($HAuCl_4$) and sodium borohydride ($NaBH_4$) were obtained from Showa. Ovalbumin (OVA) and anti-ovalbumin (anti-OVA) were obtained from Sigma-Aldrich. Mouse IgG and goat anti-mouse IgG antibody were obtained from Jackson ImmunoResearch (Baltimore, MD). All the aqueous solutions were in deionized water which was from a Millipore (Billerica, MA) Milli-Q water purification system with a resistance of 18.2 MΩ. Multimode silica optical fiber (model F-MBC) was obtained from Newport (Irvine, CA) with core and cladding diameters in 400 and 430 μm, respectively.

Microchip Construction. The sensor chip was composed of two pieces of cyclic olefin copolymer (COC) slides. These two slides had dimensions 2.5 cm × 5 cm × 0.2 cm and were produced via an injection molding process developed in our group.[19,27] The bottom slide had a microchannel with both a depth and width of 800 μm. After the top and bottom slides were bonded, the sensing region of the unclad segment (2 cm) of an optical fiber (8 cm) was placed in the microchannel and the empty spaces at both ends were sealed. The top slide contained two small holes as inlet and outlet ports to connect with sample introduction and purging tubes. The imbedded photograph in Figure 1A shows the COC chip used in this study.

Biosensor Instruments. The sensor system was similar to the previous setup.[28] Briefly, this system is equipped with a light-emitting diode (LED) light source (model IF-E93, Industrial Fiber Optic, Inc.) of peak wavelength at 532 nm, a function generator (model GFG-8225A, GW Instek) to module the output light of LED at 1 kHz, a photorecevier (model 2100, New Focus), and a lock-in amplifier (model 7225R, Signal Recovery) to improve the signal-to-noise ratio of the monitored signal. The schematic illustration of this biosensor system is shown in Figure 1B.

Antibody Immobilization and Detection. Spherical Au nanoparticles were produced via the procedures described previously.[10] The nanoparticles were self-assembled on the unclad segment, i.e., the sensing region, of the optical fiber. The nanoparticles were functionalized stepwise as follows. First, MUA (2 mM) and MCH (2 mM) were mixed at a volume ratio of 1:4 in ethanol solution. The unclad segment was then immersed in the ethanol solution for 18 h under room temperature to cover with a mixed self-assembled monolayer

dx.doi.org/10.1021/ac302590n | *Anal. Chem.* 2013, 85, 245−250

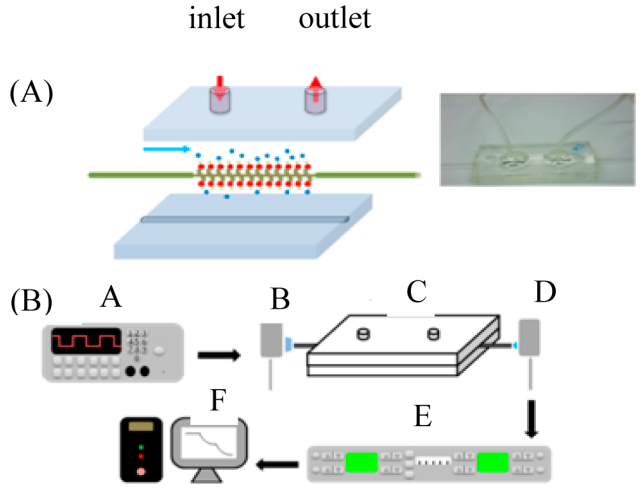

Figure 1. (A) Schematic representation of a COC chip with the unclad functionalized fiber segment sealed between the bottom slide containing one flow chamber and the top slide containing inlet and outlet ports. The inset shows a photograph of the chip. (B) The experimental setup used for the FOPPR sensing system and its working principle. The setup consists of (A) function generator, (B) light-emitting diode, (C) FOPPR sensor chip, (D) photodiode, (E) lock-in amplifier, and (F) computer.

(SAM) of MUA and MCH. When the full monolayer coverage was accomplished, the fiber was finally rinsed with ethanol and dried with nitrogen gas. Next, the carboxylic group of MUA in the mixed SAM was activated when the unclad fiber was immersed into an aqueous solution of EDC (0.5 M) and NHS (0.1 M) for 2 h. Upon the activation of the carboxylic group, the segment was immersed into a sodium acetate solution (pH 4) containing OVA at 1 mg/mL for 2 h or immersed into a PBS solution (pH 7.2) containing mouse IgG at 0.1 mg/mL for 2 h. The nonreacted carboxylic group of MUA was capped by injecting ethanolamine solution (1 M) into the microchannel for 30 min. The OVA- or mouse IgG-covered surface finally was rinsed thoroughly with phosphate-buffered saline (PBS) solution (pH 7.4) prior to use. When a solution of an anti-OVA or anti-mouse IgG was filled into the microhannel, the sensing segment of the optical fiber coated with the probe dock with the antibody molecules via diffusion to reach the surface, resulting in the intensity change of the PPR signal. The temporal intensity evolution was monitored to record the antigen−antibody binding kinetics. Moreover, the FOPPR biosensor was able to be regenerated with glycine buffer (10 mM), of which the pH value was adjusted to 1.8 with HCl solution (1 M). At least five chips were prepared to replicate each measurement data set of monitoring the above antibody binding kinetics (anti-OVA and anti-IgG).

Theory of Measuring Kinetics Constants. As eq 1 describes in the introduction, each antibody Ab binds with one immobilized antigen Ag at the gold nanoparticle surface on the unclad fiber segment. The association and dissociation constants of forming antibody−antigen complex are k_a and k_d, respectively. In the beginning of a binding reaction, when the antibody molecules are not yet depleted even in the regime near the binding surface, the antibody concentration remains virtually unchanged and the same as the bulk. When this condition is valid, the binding kinetics is controlled by the association and dissociation rate constants to neglect the transport of antibody molecules. Under this circumstance, the formation rate of product complex is described using the following pseudo-first-order rate equation

$$\frac{d[\text{Ag: Ab}]}{dt} = k_a[\text{Ab}]([\text{Ag}]_{max} - [\text{Ag: Ab}]) - k_d[\text{Ag: Ab}] \quad (2)$$

where [Ag:Ab] and [Ab] represent the concentrations of product complex on the fiber surface and antibody solution, respectively, and $[\text{Ag}]_{max}$ is the concentration of all available binding sites on the fiber surface prior to binding. Therefore, $[\text{Ag}]_{max} - [\text{Ag:Ab}]$ indicates the available binding sites on the fiber surface when the binding is proceeding. This equation describes the temporal concentration change of product complex. The amount of complex is determined by eq 2, where the first term accounts for the binding reaction to unoccupied surface binding sites near the fiber surface with the association rate constant k_a and the second term deducts the continuous dissociation of antibody with the dissociation rate constant k_d due to the finite lifetime of the complex ($t_{lifetime} = k_d^{-1}$). While the binding is proceeding, the change of available binding sites on the fiber surface can be recorded by the FOPPR sensor signal, which is the intensity of propagating light after interaction with the immobilized gold nanoparticles and exiting the fiber. The concentration of the product complex in eq 2 can be related to the light intensity $I_{(t)}$ as follows

$$\frac{dI_{(t)}}{dt} = k_a C(I_{min} - I_{(t)}) - k_d I_{(t)} \quad (3)$$

where I_{min} is the intensity of the sensor signal when all binding sites are saturated with antibody molecules and C is the antibody concentration in the sample.

Rearranging eq 3, we obtained one Bernoulli equation:

$$\frac{dI_{(t)}}{dt} = k_a C I_{min} - (k_a C + k_d) I_{(t)} \quad (4)$$

The solution of eq 4 is the following:

$$I_{(t)} = \frac{k_a C I_{min}}{k_a C + k_d} + \left(I_o - \frac{k_a C I_{min}}{k_a C + k_d}\right) e^{-(k_a C + k_d)t} \quad (5)$$

When time (t) goes to infinity, the binding reaction reaches its steady state. Therefore, the signal intensity becomes unchanged, that is, dI/dt equals to zero. Under this condition, eq 4 becomes

$$k_a C I_{min} = (k_a C + k_d) I_{eq} \quad (6)$$

where I_{eq} stands for the steady state-signal intensity. Having been rearranged, eq 6 becomes

$$I_{eq} = \frac{k_a C I_{min}}{k_a C + k_d} \quad (7)$$

Using eq 7 to substitute into the eq 5, the temporal relation of signal intensity can be expressed as eq 8

$$I_{(t)} = I_{eq} + (I_o - I_{eq}) e^{-(k_a C + k_d)t} \quad (8)$$

where I_o represent the initial signal intensity in a buffer blank when all binding sites are available and I_{eq} represents the steady state intensity in a sample. Equation 8 can be rearranged and converted into logarithm form as follows:

dx.doi.org/10.1021/ac302590n | Anal. Chem. 2013, 85, 245−250

$$\ln\left[\frac{(I_{(t)} - I_{eq})}{(I_o - I_{eq})}\right] = -(k_a C + k_d)t \quad (9)$$

Hence, the logarithm value $\ln[(I_{(t)} - I_{eq})/(I_o - I_{eq})]$ in eq 9 becomes a linear function with respect to time (t) when the concentration term C is specified. Therefore, using several given original concentrations C_1, C_2, ..., and C_n, the resulting slope values $S(C_1)$, $S(C_2)$, ..., and $S(C_i)$, respectively, can be used to estimate unknown parameters, such as k_a and k_d, via the regression procedures based on the linear relation between slope and concentration.

$$S(C_i) = k_a C_i + k_d \quad (10)$$

RESULTS AND DISCUSSION

As described in the Materials and Methods, to improve the feasibility of our idea to estimate k_a and k_d, binding kinetics measurements using anti-OVA samples of different concentrations to react with immobilized OVA were carried out with the FOPPR sensor. The other binding model using goat anti-mouse IgG to react with immobilized mouse IgG was also investigated. Figure 2, parts A and B, show the binding results of OVA/anti-OVA and IgG/anti-IgG reactions recorded with FOPPR signals, respectively.

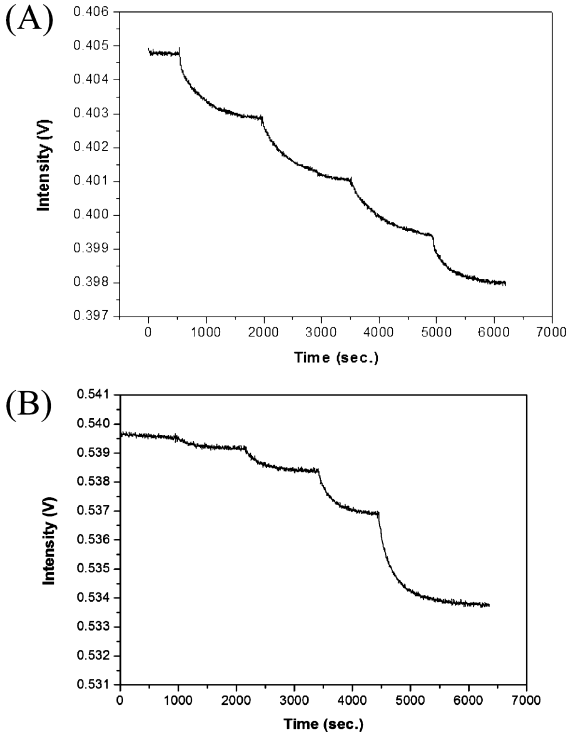

Figure 2. Temporal sensor signal curves of (A) anti-OVA samples (67, 134, 268, and 536 nM) reacted with immobilized OVA; (B) goat anti-mouse IgG samples (1.3, 5.2, 10.4, and 20.8 nM) reacted with immobilized IgG.

Since the binding kinetics model derived from eq 2 is valid only when the binding is just initiated, the time duration must be short in order to use the linear relation in eq 9. Parts A and B of Figure 3 show two typical initial curves of logarithm value in eq 9 versus time during the first 10 s using anti-OVA samples of concentrations 67 and 134 nM, respectively. The linearity of

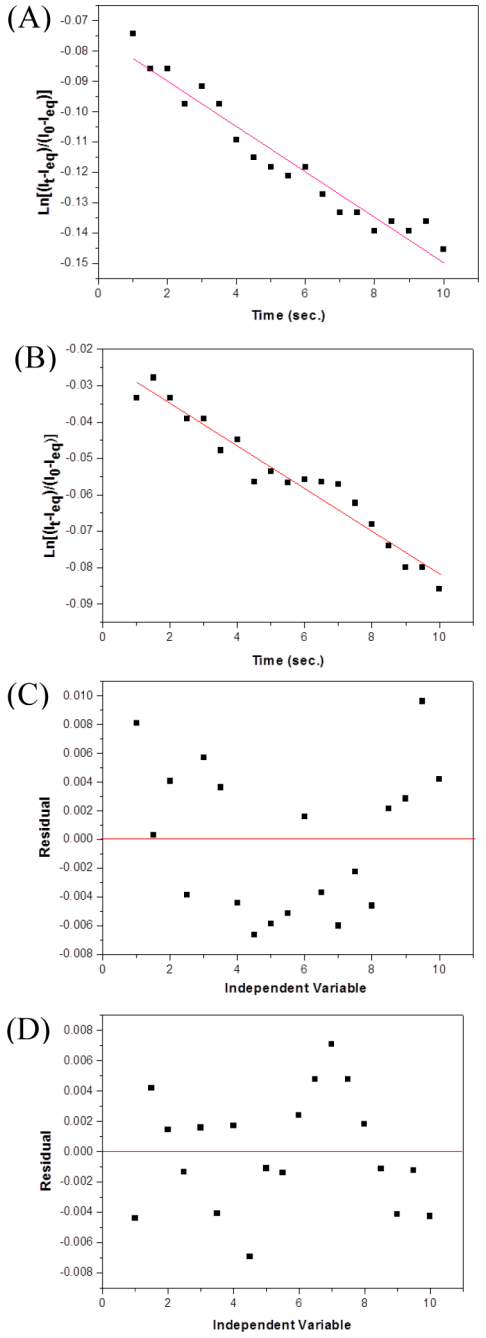

Figure 3. Regression lines of the plots of the logarithm value in eq 9 versus time for anti-OVA at a concentration of (A) 67 nM (correlation coefficient $R = 0.97$) and (B) 134 nM ($R = 0.97$). Parts C and D show the residuals analysis of the plots in parts A and B, respectively.

curves in Figure 3 is verified with high correlation coefficients ($R = 0.97$), and the residuals analyses are respectively shown Figure 3C,D. Besides, using the data in Figure 3A, the ratio of standard error to the average of logarithm value in y-axis, SE/$[y]$, is only 4.5%. When using the other four different chips to acquire binding kinetics data, the ratios of SE/$[y]$ are all within 5%, which are 2.2%, 3.7%, 1.9%, and 1.8%, respectively. This minor chip-to-chip variation illustrates that the reproducibility of this method is suitable. Similarly, the ratios of SE/$[y]$ using other concentrations of anti-OVA are all within 9% (data not shown), which demonstrates adequate reproducibility between different chips, too. The data treatment using anti-IgG result in

dx.doi.org/10.1021/ac302590n | Anal. Chem. 2013, 85, 245−250

Table 1. Association Rate Constant (k_a) and Dissociation Rate Constant (k_d) of Anti-Ovalbumin (Anti-OVA) and Ovalbumin (OVA) Binding System Measured with Various Methods[a]

k_a (M^{-1} s^{-1})	k_d (s^{-1})	K_f (M^{-1})	ref
$(1.45 \pm 0.2) \times 10^6$	$(2.97 \pm 0.6) \times 10^{-2}$	$(5.05 \pm 1.3) \times 10^7$	this study
5.25×10^6	8.00×10^{-2}	6.70×10^7	33
1.30×10^6	2.00×10^{-4}	6.70×10^9	20

[a]The measurement uncertainty in this study is estimated with the binding kinetics data using five FOPPR chips.

Table 2. Association Rate Constant (k_a) and Dissociation Rate Constant (k_d) of Anti-IgG and IgG Binding System Measured with Various Methods[a]

k_a (M^{-1} s^{-1})	k_d (s^{-1})	K_f (M^{-1})	ref
$(7.21 \pm 0.4) \times 10^3$	$(2.97 \pm 0.1) \times 10^{-3}$	$(2.43 \pm 0.2) \times 10^6$	this study
6.50×10^5	2.10×10^{-2}	3.10×10^7	29
1.06×10^5	2.49×10^{-4}	4.27×10^8	30

[a]The measurement uncertainty in this study is estimated with the binding kinetics data using five FOPPR chips.

comparable reproducibility, where the ratios of SE/[y] are all within 6% (data not shown).

Using the slopes of the linear curves in Figure 3, an association rate constant k_a and a dissociation rate constant k_d of 6.94×10^3 M^{-1} s^{-1} and 7.17×10^{-3} s^{-1}, respectively, for OVA binding with anti-OVA are obtained. Similarly, the association and dissociation rate constants of IgG binding with anti-IgG are estimated as 1.26×10^6 M^{-1} s^{-1} and 3.84×10^{-2} s^{-1}, respectively. Besides, the formation constants of the binding systems are calculated with the ratio of k_a to k_d,

$$K_f = \frac{k_a}{k_d} \tag{11}$$

Table 1 lists the results of kinetic constants k_a and k_d, and the formation constant K_f using anti-OVA and OVA binding model system in this study and previously reported values obtained with SPR sensors.[29,30] The dense polymer coating layer on the SPR chip has been suggested to present a few problems, such as retention effect and rebinding.[31,32] When the detected biomolecules are large, the determined association constants by SPR are often overestimated.[33] Because of this dense layer on the SPR chips, the detected biomolecules, which diffuse into this layer to interact with immobilized probes, are hindered by the coating polymer. As a result, these detected biomolecules are difficult to diffuse out of the layer. Therefore, these detected biomolecules are stacked inside the coating layer, since these biomolecules are easier to diffuse into rather than diffuse out of this layer, especially when their sizes are large. Such sample stacking causes the rebinding of detected biomolecules, thus altering the binding kinetics and resulting in overestimated association constants. Since anti-OVA are large proteins (MW 150 kDa), the k_a measured with SPR sensors in Table 1 are somewhat higher than the constant measured by the FOPPR sensor in this study, which can be understood by the rebinding mechanism mentioned above. On the other hand, the dissociation kinetics is a first-order reaction which is independent of the local concentration inside the coating layer. The rebinding of detected biomolecules only has minor effects in dissociation.[34] As predicted, the k_d in the first reference in Table 1[29] is close to the value in this study. (The k_d in the other reference[30] is estimated with a different mathematical model.) Similarly, Table 2 shows the estimated kinetic constants k_a and k_d and the formation constant K_f using anti-IgG and IgG binding model system in this study and published literature.[20,33] Both the k_a and k_d data in the first reference listed in this table,[33] obtained with correlation fluorescence spectroscopy method using both free anti-IgG and IgG, are close to the measured values in this study. This fluorescence method reports the binding kinetics when anti-IgG and IgG are in contact with each other via diffusion in solution. Since there is no sample stacking occurring, the measured k_a is not expected to be overestimated. There should also be no sample stacking problem in the other data set obtained with amperometric method using immobilized anti-IgG on the electrode.[20] The association rate constant k_a reported using the amperometric method is close to the value in this study. However, other polarization effects on the electrode surface negatively biased the dissociation rate constant k_d.

CONCLUSIONS

Under the assumption of pseudo-first-order approximation, when each antibody in the loaded sample binds with one immobilized antigen on the FOPPR sensing fiber segment, we use eq 1 to derive a theoretical model to facilitate the measurement of binding association and dissociation constants by monitoring the initial binding kinetics curve using FOPPR signals.

When the differences in device and mathematical model are taken into considerations, the binding kinetic rate constants estimated with the FOPPR system and the procedures based on the pseudo-first-order model in this study are consistent with the reported values in the literature. Therefore, this work has successfully demonstrated the feasibility of using a FOPPR sensor to estimate the binding kinetic constants.

AUTHOR INFORMATION

Corresponding Author

*E-mail: chescw@ccu.edu.tw (S.-C.W.); chelkc@ccu.edu.tw (L.-K.C.).

Notes

The authors declare no competing financial interest.

ACKNOWLEDGMENTS

This research was financial supported by National Science Council, Taiwan (ROC) and National Chung Cheng University through Grant numbers NSC 97-2113-M-194-008-MY3 and NSC 100-2120-M-194-005-CC1.

REFERENCES

(1) Cheng, S.-F.; Chau, L.-K. *Anal. Chem.* **2003**, *75*, 16.
(2) Haes, A. J.; P. H., W.; Chang, L.; Klein, W. L.; Van Duyne, R. P. *Nano Lett.* **2004**, *4*, 1029.
(3) Raschke, G.; Kowarik, S.; Franzl, T.; So1nnichsen, C.; Klar, T. A.; Feldmann, J. *Nano Lett.* **2003**, *3*, 935.
(4) Cui, Y.; Wei, Q.; Park, H.; Lieber, C. M. *Science* **2001**, *293*, 1289.
(5) Besteman, K.; Lee, J.-O.; Wiertz, F. G. M.; Heering, H. A.; Dekker, C. *Nano Lett.* **2003**, *3*, 727.
(6) Chen, H.; Kou, X.; Yang, Z.; Wang, W. N. J. *Langmuir* **2008**, *24*, 5233.
(7) Jensen, T. R.; Duval, M. L.; Kelly, K. L.; Lazarides, A. A.; Schatz, G. C.; Duyne, R. P. V. *J. Phys. Chem. B* **1999**, *103*, 9846.
(8) Nath, N.; Chilkoti, A. *Anal. Chem.* **2002**, *74*, 504.
(9) Cheng, S. F.; Chau, L. K.; Pao, K. C. *J. Biomed. Nanotechnol.* **2005**, *1*, 143.
(10) Chen, C. D.; Cheng, S. F.; Chau, L. K.; Wang, C. R. *Biosens. Bioelectron.* **2007**, *22*, 926.
(11) Yonzon, C. R.; Jeoung, E.; Zou, S.; Schatz, G. C.; Mrksich, M.; Duyne, R. P. V. *J. Am. Chem. Soc.* **2004**, *126*, 12669.
(12) Chau, L.-K.; Lin, Y.-F.; Cheng, S.-F.; Lin, T.-J. *Sens. Actuators, B* **2006**, *113*, 100.
(13) Rasooly, A. *J. Food Prot.* **2001**, *64*, 37.
(14) Haes, A. J.; Zou, S.; Schatz, G. C.; Duyne, R. P. V. *J. Phys. Chem. B* **2004**, *108*, 109.
(15) DeGrandpre, M. D.; Burgess, L. W. *Anal. Chem.* **1988**, *60*, 2582.
(16) Stanley, C.; Lew, A. M.; Steward, M. W. *J. Immunol. Methods* **1983**, *64*, 119.
(17) Johnstone, R. W.; Andrew, S. M.; Hogarth, M. P.; Pietersz, G. A.; McKenzie, I. F. C. *Mol. Immunol.* **1990**, *27*, 327.
(18) Kima, H.-J.; Shelver, W. L.; Li, Q. X. *Anal. Chim. Acta* **2004**, *509*, 111.
(19) Hall, D. R.; Winzor, D. J. *Anal. Biochem.* **1997**, *244*, 152.
(20) Ivnitski, D.; Wolf, T.; Solomon, B.; Fleminger, G.; Rishpon, J. *Bioelectrochem. Bioenergetics* **1998**, *45*, 27.
(21) Okahata, Y.; Kawase, M.; Niikura, K.; Ohtake, F.; Furusawa, H.; Ebara, Y. *Anal. Chem.* **1998**, *70*, 1288.
(22) Edwards, P. R.; Maule, C. H.; Leatherbarrow, R. J.; Winzor, D. J. *Anal. Biochem.* **1998**, *263*, 1.
(23) Wong, M.-S.; Fong, C.-C.; Yang, M. *Biochim. Biophys. Acta* **1999**, *1432*, 293.
(24) Glaser, R. W. *Anal. Biochem.* **1993**, *213*, 152.
(25) Schuck, P.; Minton, A. P. *Anal. Biochem.* **1996**, *240*, 262.
(26) Myszka, D. G.; He, X.; Dembo, M.; Morton, T. A.; Goldstein, B. *Biophys. J.* **1998**, *75*, 583.
(27) Chuang, Y.; Lee, C.-Y.; Lu, S.-H.; Wang, S.-C.; Chau, L.-K.; Hsieh, W.-H. *Anal. Chem.* **2010**, *82*, 1123.
(28) Hsu, W. T.; Hsieh, W. H.; Cheng, S. F.; Jen, C. P.; Wu, C. C.; Li, C. H.; Lee, C. Y.; Li, W. Y.; Chau, L. K.; Chiang, C. Y.; Lyu, S. R. *Anal. Chim. Acta* **2011**, *697*, 75.
(29) Oda, M.; Uchiyama, S.; Robinson, C. V.; Fukui, K.; Kobayashi, Y.; Azuma, T. *FEBS J.* **2006**, *273*, 1476.
(30) Brogan, K. L.; Shin, J. H.; Schoenfisch, M. H. *Langmuir* **2004**, *20*, 9729.
(31) Schuck, P. *Biophys. J.* **1996**, *70*, 1230−1249.
(32) Goldstein, B.; Coombs, D.; He, X.; Pineda, A. R.; Wofsy, C. *J. Mol. Recognit.* **1999**, *12*, 293−299.
(33) Varghese, L.; Sinha, R.; Irudayaraj, J. *Anal. Chim. Acta* **2008**, *625*, 103.
(34) Fong, C.-C.; Wong, M.-S.; Fong, W.-F.; Yang, M. *Anal. Chim. Acta* **2002**, *456*, 201.